Chemical Science

ROYAL SOCIETY OF CHEMISTRY

EDGE ARTICLE

View Article Online
View Journal | View Issue

Cite this: *Chem. Sci.*, 2025, **16**, 2215

All publication charges for this article have been paid for by the Royal Society of Chemistry

Tuning the interlayer stacking of a vinylene-linked covalent organic framework for enhancing sacrificial agent-free hydrogen peroxide photoproduction†

Qiujian Xie,‡[a] Anqi Chen,‡[a] Xiaofeng Li,[a] Chen Xu,[a] Shuai Bi,[b] Weijie Zhang,[c] Juntao Tang,[a] Chunyue Pan,[a] Fan Zhang *[b] and Guipeng Yu *[a]

The layer-stacking mode of a two-dimensional (2D) material plays a dominant role either in its topology or properties, but remains challenging to control. Herein, we developed alkali-metal ion-regulating synthetic control on the stacking structure of a vinylene-linked covalent triazine framework (termed sp^{2}c-CTF) for improving hydrogen peroxide (H_2O_2) photoproduction. Upon the catalysis of EtONa in Knoevenagel polycondensation, a typical eclipsed stacking mode (sp^{2}c-CTF-4@AA) was built, while a staggered one (sp^{2}c-CTF-4@AB) was constructed using LiOH. The AB stacking might be induced by the Li^+ promoted Lewis acid–base interactions with the nitrogen atoms of *s*-triazine units which would endow the *s*-triazine units with a charged state and enlarge the total crystal stacking energy. Specifically, the shift in the stacking mode speeds up electron transfer within each layer and along interlayers, thereby improving the photocatalytic activity. sp^{2}c-CTF-4@AB features superior activity over the eclipsed stacking counterpart (sp^{2}c-CTF-4@AA) in sacrificial agent-free H_2O_2 generation, comparable to the state-of-the-art COF photocatalysts, which has not been demonstrated in this field before. This work demonstrates that regulating the interlayer-stacking mode of COFs can endow them with high photocatalytic activity, further inspiring the development of heterogeneous catalysis.

Received 23rd September 2024
Accepted 16th December 2024

DOI: 10.1039/d4sc06451h

rsc.li/chemical-science

Introduction

Two-dimensional (2D) materials, including graphene, hexagonal BN, MoS_2, *etc.*, have been reported and extensively studied in various applications such as optoelectronics, spintronics, catalysts, chemical and biological sensors, supercapacitors, solar cells, and lithium-ion batteries for their distinct properties.[1–4] Controlling the stacking mode of 2D materials endows them with unconventional mechanical, photoelectrical, and chemical properties.[5–7] For instance, the evolution of monolayer molybdenum disulfide (ML-MoS_2) from the 2H phase (AB-stack) to the 1T phase (ABC-stack) gave significantly different conductivity.[8,9] 2D covalent organic frameworks (COFs) have emerged as a new class of materials with defined molecular stacking, large surface areas and open regular channels, featuring extended molecular sheets interacting through non-covalent interactions like π–π and van der Waals forces.[10–13] The pioneer 2D COF was disclosed by Yaghi *et al.* in 2005, which features an unusual AB stacking mode through boronate/boroxine polycondensation chemistry.[14] However, most known 2D COFs are AA stacked, and the known reports are focused on exploring available synthetic methods for 2D COFs, reticulating building blocks, or establishing new covalent linkages and topologies for task-specific functionalities and applications. The topology and properties of 2D COFs were mainly tailored through in-plane molecular structures, but seldom by the vertical stacking modes.[15–18] Several limited pioneering efforts including judicious regulation of building blocks, and catalyst-triggered (like CF_3SO_3H) or solvent-assisted methods have been found to be effective in weakening the attraction of π–π stacking layers and facilitating interlayer sliding.[19–21]

More recently, numbered vinylene-linked covalent organic frameworks (sp^{2}c-COFs) have been developed *via* Knoevenagel or aldol condensation routes, and they have exhibited high chemical stability and attractive photocatalytic activity due to their

[a]*Hunan Key Laboratory of Micro & Nano Materials Interface Science, College of Chemistry and Chemical Engineering, Central South University, Changsha 410083, P. R. China. E-mail: gilbertyu@csu.edu.cn*

[b]*State Key Laboratory of Metal Matrix Composites, School of Chemistry and Chemical Engineering, Shanghai Jiao Tong University, Shanghai 200240, P. R. China. E-mail: Fan-zhang@sjtu.edu.cn*

[c]*Hunan Provincial Key Laboratory of Environmental Catalysis & Waste Recycling, College of Materials and Chemical Engineering, Hunan Institute of Engineering, Xiangtan 411104, P. R. China*

† Electronic supplementary information (ESI) available. See DOI: https://doi.org/10.1039/d4sc06451h

‡ Q. X. and A. C. contributed equally to this work.

robust and fully π-conjugated backbones.[22–24] The photocatalytic transformations enabled by sp^2c-COFs, such as photocatalytic H_2O_2 generation, provide an alternative approach to dismiss the disadvantages (*e.g.*, high energy consumption, safety risks)[25,26] of the traditional anthraquinone method. However, very limited structures or topologies of sp^2c-COFs have been developed so far, and unveiling the relationship between the bulk structure and photocatalytic activity remains a highly challenging subject. Herein, we report an alkali-metal ion-regulating strategy to control the stacking structure of a vinylene-linked covalent triazine framework (sp^2c-CTF-4) during the Knoevenagel polycondensation. An eclipsed AA stacking mode (denoted as sp^2c-CTF-4@AA) was achieved by applying sodium ethoxide (EtONa) as the catalyst. A staggered stacking mode (sp^2c-CTF-4@AB) was formed upon catalysis of lithium hydroxide (LiOH). Such phenomena were ascribed to the enlarged total crystal stacking energy from the coordination of Li^+ ions to the nitrogen atoms of the *s*-triazine unit during the growth of frameworks. The two stacking-mode COFs showed significantly different physical properties and photocatalytic activities toward the production of H_2O_2 under visible light irradiation. Because of the much stronger capability in separation and transport of photogenerated charge carriers, the rate of H_2O_2 generation of sp^2c-CTF-4@AB can reach 2758 μmol h^{-1} g^{-1}, which is unprecedentedly 2.7 fold that of the eclipsed stacking counterpart without adding any sacrificial agent. This finding provides new guidance in the design and synthesis of efficient and stable heterogeneous catalysts for H_2O_2 production.

Results and discussion

The vinylene (–CH=CH–) connected covalent triazine framework (sp^2c-CTF-4) was synthesized through the Knoevenagel condensation between TMT and TFPB under selected conditions (Fig. 1a). The sp^2c-CTF-4@AA sample with an eclipsed stacking mode was synthesized in a binary solvent of *o*-dichlorobenzene/*n*-butanol (3/7 v/v) under the catalysis of sodium ethoxide (EtONa). The staggered-stacking sp^2c-CTF-4@AB was prepared under optimized solvothermal conditions of dimethyl formamide/*o*-dichlorobenzene/methanol (3/1/0.2 v/v/v) in the presence of lithium hydroxide (LiOH) (detailed in the synthesis section of the ESI†). sp^2c-CTF-4@AA is obtained as a pale-yellow powder (yield: 87%), whereas the staggered-stacking sp^2c-CTF-4@AB is yellow (fluffy, yield: 86%). The crystallinity of the resultant frameworks was revealed by PXRD measurements. sp^2c-CTF-4@AA shows clear characteristic peaks at 5.9°, 10.2°, and 11.7°, representing the (100), (110) and (200) facets, respectively, for an eclipsed stacking model (Fig. 1b). The peak at 25.3° corresponds to the layer-to-layer eclipsed stacking distance of 3.43 Å (001). In contrast, the experimental PXRD results for sp^2c-CTF-4@AB, including the number, position, and strength of peaks, matched well with a staggered stacking model (PM space group, unit cell parameters: $a = b = 17.53$, $c = 3.1$, $\alpha = \beta = 90°$, and $\gamma = 120°$). The signal observed at 21.5° (Fig. 1c) clearly indicates the formation of Li–N interaction around the triazine units.[27,28] The chemical structure, porosity, morphology, and photoelectric properties of two sp^2c-CTF-4

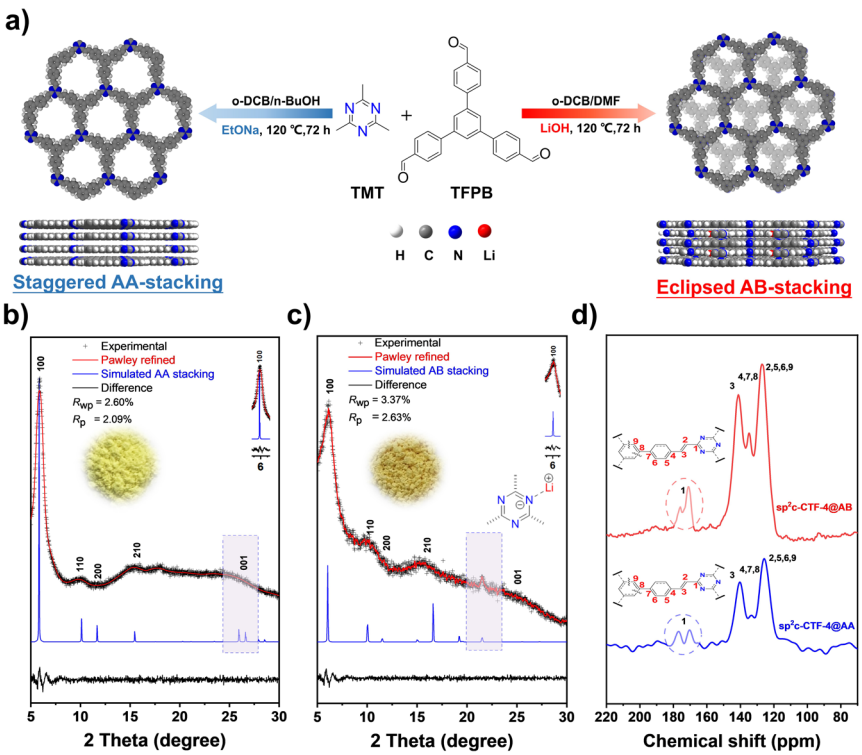

Fig. 1 (a) Schematic diagram for the synthesis of sp^2c-CTF-4 and views of the corresponding refined 2D crystal structure; PXRD patterns of (b) sp^2c-CTF-4@AA and (c) sp^2c-CTF-4@AB; comparison between the experimental (black cross) and Pawley refined (red line) profiles, the simulated patterns for AA and AB stacking mode (blue line); (d) ^{13}C CP/MAS solid-state NMR spectra of sp^2c-CTF-4@AA and sp^2c-CTF-4@AB.

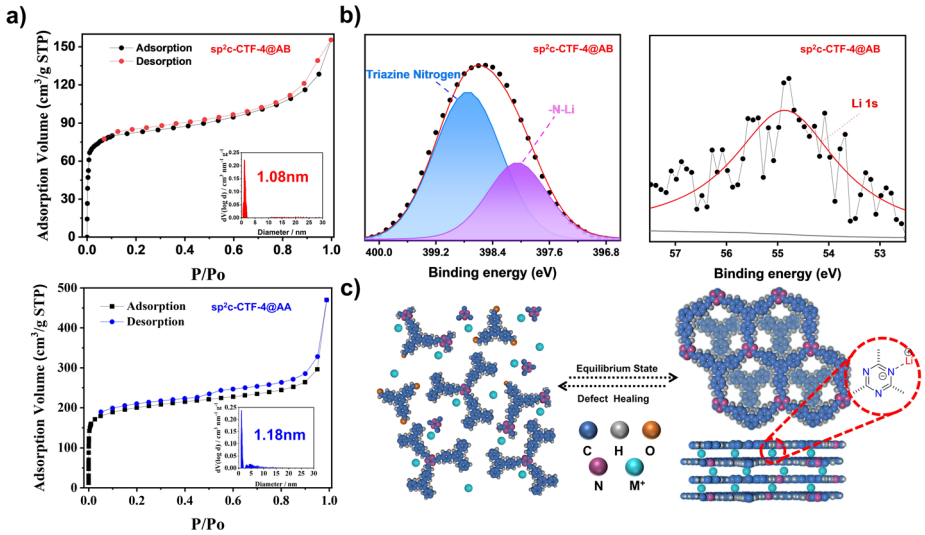

Fig. 2 (a) (top) Nitrogen adsorption (black) and desorption (red) isotherms of sp^{2}c-CTF-4@AB ((inset) pore size distribution curve of sp^{2}c-CTF-4@AB); (bottom) nitrogen adsorption (black) and desorption (blue) isotherms of sp^{2}c-CTF-4@AA ((inset) pore size distribution of sp^{2}c-CTF-4@AA); (b) XPS spectra of N 1s (left) and Li 1s (right) for sp^{2}c-CTF-4@AB; (c) plausible formation mechanism for sp^{2}c-CTF-4@AB.

samples were characterized and compared. The formation of olefin (–C=C–) linkage was proved by Fourier transform infrared (FT-IR) spectra through the emergence of vinylene stretching vibration (1630 cm^{-1}). Both of the two samples show structural similarity without clear distinction on the absorbance intensity location of specific peaks (Fig. S1†).[29] Besides, the band at 1628 cm^{-1} in Raman spectroscopy further proves the formation of C=C linkages for the as-synthesized frameworks (Fig. S2†). High-resolution TEM (HR-TEM) images of sp^{2}c-CTF-4 further confirmed the aligned porous structure (Fig. S3†). A solid ^{13}C cross-polarization magic angle spinning nuclear magnetic resonance (CP-MAS NMR) spectrum (Fig. 1d), in which all prominent signals are well consistent with the proposed polymer structure, further confirms the successful polycondensation. Besides, different aggregation structures of 2D COFs can be investigated using ^{13}C CP/MAS solid-state NMR. Compared with sp^{2}c-CTF-4@AA, the peak intensity of the triazine carbon at 176.2 ppm for sp^{2}c-CTF-4@AB is sharply attenuated, indicating that the intimate interactions between the neighboring layers of the sp^{2}c-CTF-4@AB are weakened, and the change in the fine chemical environment further proves the formation of the AB stacking mode.[30] N_2 sorption isotherm measurements were conducted to probe the porous structure of the obtained frameworks (Fig. 2a). Based on the nonlocal density functional theory (NLDFT) model, pore size distribution (PSD) was evaluated. sp^{2}c-CTF-4@AA delivers a high BET surface area of 752 m^2 g^{-1} with a dominant pore diameter at 1.18 nm. In contrast, a lower BET surface area of 278 m^2 g^{-1} for sp^{2}c-CTF@AB, and a slightly narrow dominant pore width in the PSD curve suggests the presence of meandering channels and certain inaccessible pore volumes for nitrogen probes, probably ascribed to its relatively lower crystallinity and the presence of Li$^+$ within its lattice.

A few reports have shown that the phase conversion of staggered modes to eclipsed ones in COFs was triggered by certain synthetic conditions. The synthetic conditions indeed dominate the polymorph formation and crystalline evolution.[31,32] Of particular interest is the possible mechanism for the formation of the AB-stacking structure. In our case, N atoms of the triazine unit with a lone pair of electrons appear to be potential Lewis-base sites, coordinating with Lewis-acid sites (metal ions). The possible interaction between the triazine unit and Li$^+$ was probed *via in situ* ^{1}H-NMR spectroscopic measurements on model compounds like 2,4,6-trimethyl-1,3,5-triazine (TMT). After mixing with various concentrations of LiOH·H_2O, the ^{1}H NMR signals at 2.60 ppm for hydrogens of the methyl group in TMT transfer to the high field (2.46–2.50 ppm). This indicates that there would be an interaction between Li$^+$ and the triazine unit (Fig. S4†). X-ray photoelectron spectroscopy (XPS) measurements were further conducted to distinguish the chemical state of nitrogen atoms. The N 1s spectra of sp^{2}c-CTF-4@AB are deconvoluted into a single peak located at 398.7 eV, which was attributed to triazine N. An additional peak is found at 398.1 eV for the N 1s signal of the N–Li peak. Accordingly, the deconvoluted peak in the Li 1s spectrum could be assigned to the Li–N coordinate bond (Fig. 2b), further identifying the Li–N interaction.[33,34] Notably, inductively coupled plasma-atomic emission spectrometry (ICP-AES) results (residual Li$^+$: 0.03 wt%) indicate that each triazine ring would be coordinated with one Li$^+$ in a cell. The Na$^+$ content of sp^{2}c-CTF-4@AA based on ICP-AES analysis is merely 0.01 wt%. Therefore, the residual Na$^+$ would exert an almost negligible effect on the crystallinity evolution of our frameworks.

To unveil the stability of different stacking modes, first-principles calculations were carried out (Fig. S5 and 6†). Total energy calculations show that the Li coordination strengthens the stability of sp^{2}c-CTF-4@AB by Li–N interaction.[35] The corresponding topology of sp^{2}c-CTF-4@AB was modeled with Pawley refinement, exhibiting a staggered stacking model with good R factors (R_p = 3.37%, R_{wp} = 2.63%). DFT calculations

reveal that such stacking mode also exhibits lower energy than those of sp^{2}c-CTF-4@AA with or without Li^+ coordination by 95.46 kcal m^{-1} or 49.58 kcal m^{-1}, respectively, which is also much lower than that of Li-free sp^{2}c-CTF-4@AB by 48.65 kcal m^{-1} (Table S1†). These results indicate that the formation of AB stacking might be induced by the Lewis acid–base interactions between Li^+ and the nitrogen atoms of *s*-triazine units. The interaction would endow the *s*-triazine units with a charged state, enlarging the total crystal stacking energy. This means there is a certain amount of electronic repulsion between sp^{2}c-CTF-4 layers, which leads to a staggered stacking mode (Fig. 2c).[36] sp^{2}c-CTF-4@AB could maintain the primary skeleton connectivity after being treated in saturated KOH methanol/water (1 : 1) solution (Fig. S7†), as revealed by XPS spectra, manifesting its relative stability.

sp^{2}c-CTF-4 samples exhibited broad visible-light absorbance extended to 600 nm in UV-visible diffuse reflectance spectra (DRS), which would be attractive for the efficient utilization of natural sunlight (Fig. 3a).[37] From the UV-vis DRS, the corresponding Tauc plot analysis exhibits optical energy band gaps of 2.67 and 2.65 eV for sp^{2}c-CTF-4@AA and sp^{2}c-CTF-4@AB, respectively (Fig. S8 and 9†). Mott–Schottky measurements were conducted to study the electronic structure and relative band positions. The positive slope indicates typical n-type semiconductor characteristics for sp^{2}c-CTF-4@AA and sp^{2}c-CTF-4@AB (Fig. S10 and S11†). Accordingly, the corresponding conduction band (CB) and valence band (VB) were calculated (Fig. 3b). The CB bottoms of both COFs lie above the potential for the O_2/H_2O_2 (+0.68 V *vs.* NHE), ensuring sufficient reduction potential for H_2O_2 generation from the ORR. In addition, the oxidation potential of sp^{2}c-CTF-4 also meet the theoretical prerequisite for the WOR to produce H_2O_2. The transient-photocurrent-response intensity of sp^{2}c-CTF-4@AB is much higher than that of sp^{2}c-CTF-4@AA, as shown in Fig. 3c. In the meantime, according to electrochemical impedance spectroscopy (EIS), the electronic conductivity of sp^{2}c-CTF-4@AB is also superior to that of sp^{2}c-CTF-4@AA (Fig. S12†). Furthermore, the PL intensity of sp^{2}c-CTF-4@AB is slightly quenched in comparison with that of sp^{2}c-CTF-4@AA (Fig. S13†), verifying a more effective suppression of photogenerated carrier recombination. More efficient separation of charge carriers and a higher interfacial charge transfer rate have been demonstrated by sp^{2}c-CTF-4@AB, which is beneficial for photocatalytic processes.[38–43] The stacking mode evolution of the as-prepared COFs led to intense differences in their photophysical properties and hence photocatalytic performance. The electron–hole pair distribution of the two frameworks was further compared by theoretical calculations (Fig. S14†). sp^{2}c-CTF-4@AB gave a significantly weaker electron–hole complexing ability than sp^{2}c-CTF-4@AA. We conjecture that the shift in the stacking pattern might allow electrons to transfer either within each layer of COFs or along the interlayers. Thus, all of this further proves that the photophysical properties of sp^{2}c-CTF-4@AB are superior to those of sp^{2}c-CTF-4@AA.

The photocatalytic H_2O_2 production measurements were carried out using sp^{2}c-CTF-4@AA and sp^{2}c-CTF-4@AB as photocatalysts in pure water and O_2 without the addition of any sacrificial reagent under visible light irradiation. sp^{2}c-CTF-4@AB showed an amazing photocatalytic H_2O_2 production performance with a production rate over 2758 μmol h^{-1} g^{-1} (Fig. 3d), whereas sp^{2}c-CTF-4@AA offered a lower H_2O_2 production rate (1020 μmol h^{-1} g^{-1}). Compared with the monomer TMT, TFPB and the model product (TST), sp^{2}c-CTF-4 showed significantly superior H_2O_2 properties, suggesting that the formation of the conjugated structure is more favourable for the generation and transport of photogenerated carriers (Fig. S15 and 16†). sp^{2}c-CTF-4@AB showed 2.7 fold better performance than sp^{2}c-CTF-4@AA, and this trend is consistent with their physical properties. In addition, sp^{2}c-CTF-4@AB produced H_2O_2 with a much better cycling performance as compared with

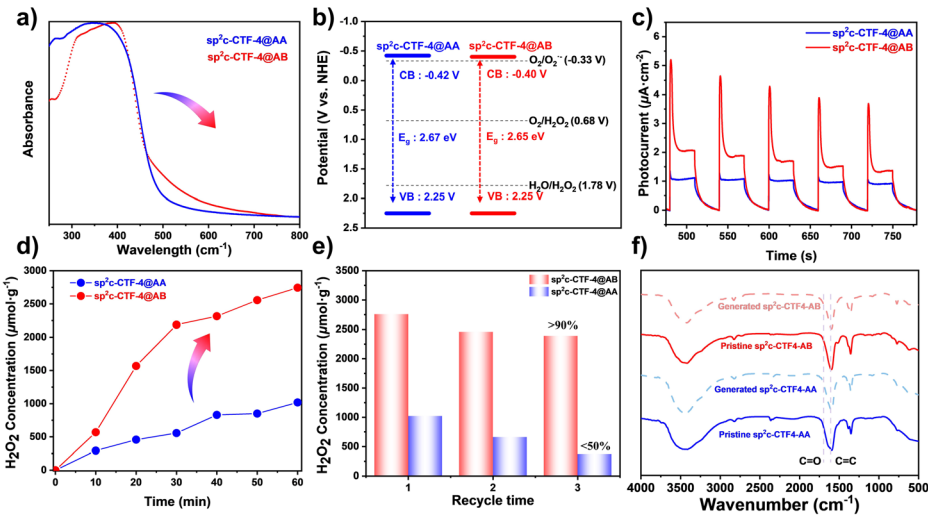

Fig. 3 (a) UV/vis DRS of sp^{2}c-CTF-4@AA and sp^{2}c-CTF-4@AB. (b) Band structures of sp^{2}c-CTF-4@AA and sp^{2}c-CTF-4@AB. (c) Chopped photocurrent density *vs.* time recorded on sp^{2}c-CTF-4@AA and sp^{2}c-CTF-4@AB at 0.6 V *vs.* RHE. (d) Time-dependent H_2O_2 photogeneration using visible light for sp^{2}c-CTF-4@AA and sp^{2}c-CTF-4@AB (5 mg catalyst in 10 mL pure water); (e) recycling H_2O_2 production on sp^{2}c-CTF-4 (reaction time: 1 h); (f) FTIR spectra of sp^{2}c-CTF-4 before and after the H_2O_2 photogeneration cycle.

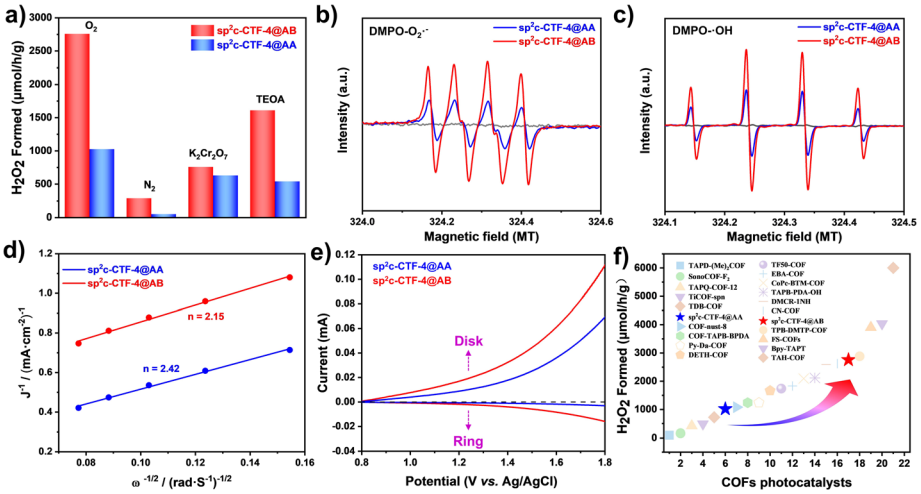

Fig. 4 (a) H_2O_2 production of sp^{2}c-CTF-4@AA and sp^{2}c-CTF-4@AB under different conditions (O_2, N_2, $K_2Cr_2O_7$, TEOA); (b) DMPO spin-trapping EPR spectra of sp^{2}c-CTF-4 for measuring $O_2^{\bullet-}$; (c) DMPO spin-trapping EPR spectra of sp^{2}c-CTF-4 for measuring $^{\bullet}OH$; (d) the Koutecky–Levich plots obtained *via* RDE measurements in phosphate buffer (pH 7) solution with continuous O_2 purging; (e) polarization curves recorded with simultaneous detection of H_2O_2 at the ring electrode at 1600 rpm; (f) summary of photocatalytic H_2O_2 evolution rates of sp^{2}c-CTF-4 and other COF-based photocatalysts.

sp^{2}c-CTF-4@AA (Fig. 3e). The IR spectra show that sp^{2}c-CTF-4 maintains good structural stability after H_2O_2 cycling performance tests (Fig. 3f). To clarify the exact H_2O_2 production process, a series of control experiments were carried out. Under high-purity nitrogen conditions (continuous ventilation to prevent the interference of oxygen), the two sp^{2}c-CTF-4 samples still have some ability to produce H_2O_2 (Fig. 4a). This means that they are likely to have a water oxidation pathway in this process. In addition, potassium dichromate ($K_2Cr_2O_7$) and triethanolamine (TEOA) are chosen as electron and hole sacrificial agents to study the H_2O_2 production capacity of the sp^{2}c-CTF-4, and the results show that both electrons and holes play important roles in this process. To probe the reactive oxygen species in the photocatalytic process, electron paramagnetic resonance (EPR) spectra were measured using DMPO as a spin-trapping agent. As illustrated in Fig. 4b and c, under visible light irradiation, typical characteristic peaks of DMPO-$O_2^{\bullet-}$ for sp^{2}c-CTF-4 were observed, indicating the production of $O_2^{\bullet-}$ intermediate species. This result further suggests that this ORR is the 2e two-step oxygen reduction pathway for H_2O_2 production ($O_2 \rightarrow O_2^{\bullet-} \rightarrow H_2O_2$) in this system. Meanwhile, DMPO-$^{\bullet}OH$ signals are detected for sp^{2}c-CTF-4 samples. In addition, the typical characteristic peaks for sp^{2}c-CTF-4@AB are significantly stronger than those for sp^{2}c-CTF-4@AA, indicating the superior ability of the former to produce both $O_2^{\bullet-}$ and $^{\bullet}OH$ intermediate species. To further elucidate the mechanism of H_2O_2 generation, more control experiments (Fig. 4d and e) were carried out. The rotating disk electrode tests show that the number of transferred electrons is 2.42 for sp^{2}c-CTF-4@AA and 2.15 for sp^{2}c-CTF-4@AB, respectively. In addition, the rotating ring disk electrode tests show that both materials could oxidize water into H_2O_2. Therefore, it can be concluded that these catalytic systems produce H_2O_2 mainly by the two-step single-electron oxygen reduction pathway ($O_2 \rightarrow O_2^{\bullet-} \rightarrow H_2O_2$) supplemented by the water oxidation pathway (Fig. S17†).

The H_2O_2 production performance of the sp^{2}c-CTF-4 photocatalyst in the presence of alkali catalysts (LiCl: 0.03% or NaCl: 0.01%) was investigated (Fig. S18†). Neither the addition of LiCl to the sp^{2}c-CTF-4@AA photocatalytic system nor the addition of NaCl to the sp^{2}c-CTF-4@AB photocatalytic system caused any obvious change in the H_2O_2 production rate. It is demonstrated that the photocatalytic activity is not influenced by free Li^+, and the performance is improved only when Li^+ *in situ* interacted with the N atoms in the *s*-triazine units during the polycondensation. Among most known COF photocatalysts for H_2O_2 production (Fig. 4f and Table S2†),[44–62] sp^{2}c-CTF-4@AB is comparable to many known COF photocatalysts, exhibiting 2.7 fold as high performance as that of sp^{2}c-CTF-4@AA. In addition, our sp^{2}c-CTF-4 photocatalysts show prominent stability under various conditions, including treatment in aqueous 35% H_2O_2, concentrated HCl (12 M), and saturated KOH methanol/water (1 : 1) solution (Fig. S19 and 20†). This stability is superior to that of SNW-4 (ref. 63) or CTF-T1 (ref. 64) (Fig. S21–24†), and is adaptable for versatile functional platforms like catalysis, sensing and separation.

Conclusions

In summary, we have established an efficient strategy to tailor the stacking mode in 2D vinylene-linked covalent triazine frameworks by regulating the base-catalyst with different alkali-metal ions during Knoevenagel polycondensation. A rare sp^{2}c-CTF example with a staggered stacking mode (sp^{2}c-CTF-4@AB) was obtained by utilizing the Lewis acid–base interactions between the Li^+ ions of the base catalyst and nitrogen atoms of *s*-triazine blocks. The evolution on stacking modes of 2D frameworks directly led to the significant difference in photophysical properties. Accordingly, they exhibited efficient but significantly different photocatalytic activities for the production of H_2O_2. sp^{2}c-CTF-4@AB shows attractive activity

with a H_2O_2 production rate of 2758 μmol h^{-1} g^{-1} due to its much stronger capability in separation and transport of photogenerated charge carriers. It is envisaged that either the in-plane molecular structure or vertical aggregation of a 2D vinylene-linked COF might play the key role in the design and exploration of a robust high-performance photocatalyst. This study may shed light on the regulation of crystalline structures for 2D COFs, and pave the way for developing smart framework materials with desirable properties and functionalities.

Data availability

The data supporting this article have been included as part of the ESI.†

Author contributions

Guipeng Yu, Fan Zhang, Chunyue Pan, and Juntao Tang proposed the idea and designed the experiments. Qiujian Xie and Anqi Chen performed the experiments and carried out the structural characterization. Xiaofeng Li helped to synthesize the materials. Shuai Bi helped with the structural characterization analysis. Weijie Zhang helped to analyse the results of photocatalytic experiments. Qiujian Xie and Anqi Chen wrote the manuscript with contributions from all the authors.

Conflicts of interest

There are no conflicts to declare.

Acknowledgements

This work was financially supported by the National Natural Science Foundation of China (no. 52173212, 52103275, and 22271188), the Science and Technology Innovation Program of Hunan Province (2024JK2074), Hunan Provincial Natural Science Foundation for Distinguished Young Scientists (2022JJ10080), the Key Science and Technology Project of Changsha (KH2301015) and the Open Sharing Fund for the Largescale Instruments and Equipment of Central South University (CSUZC202115). We acknowledge the XRD and NMR measurements by The Modern Analysis and Testing Center of Central South University, and we are grateful to the High-Performance Computing Center of Central South University for partial support of this work.

Notes and references

1 Z. Fu, X. Wang, A. M. Gardner, X. Wang, S. Y. Chong, G. Neri, A. J. Cowan, L. Liu, X. Li, A. Vogel, R. Clowes, M. Bilton, L. Chen, R. S. Sprick and A. I. Cooper, *Chem. Sci.*, 2020, **11**, 543–550.
2 S.-H. Bae, H. Kum, W. Kong, Y. Kim, C. Choi, B. Lee, P. Lin, Y. Park and J. Kim, *Nat. Mater.*, 2019, **18**, 550–560.
3 S. Zhang, T. Ma, A. Erdemir and Q. Li, *Mater. Today*, 2019, **26**, 67–86.
4 N. Mounet, M. Gibertini, P. Schwaller, D. Campi, A. Merkys, A. Marrazzo, T. Sohier, I. E. Castelli, A. Cepellotti, G. Pizzi and N. Marzari, *Nat. Nanotechnol.*, 2018, **13**, 246–252.
5 O. V. Yazyev and Y. P. Chen, *Nat. Nanotechnol.*, 2014, **9**, 755–767.
6 M. Xie, X.-R. Chen, K. Wu, Z. Lu, K. Wang, N. Li, R.-J. Wei, S.-Z. Zhan, G.-H. Ning, B. Zou and D. Li, *Chem. Sci.*, 2021, **12**, 4425–4431.
7 G. Zhao, X. Li, M. Huang, Z. Zhen, Y. Zhong, Q. Chen, X. Zhao, Y. He, R. Hu, T. Yang, R. Zhang, C. Li, J. Kong, J.-B. Xu, R. S. Ruoff and H. Zhu, *Chem. Soc. Rev.*, 2017, **46**, 4417–4449.
8 J. Zhu, Z. Wang, H. Yu, N. Li, J. Zhang, J. Meng, M. Liao, J. Zhao, X. Lu, L. Du, R. Yang, D. Shi, Y. Jiang and G. Zhang, *J. Am. Chem. Soc.*, 2017, **139**, 10216–10219.
9 Y. C. Lin, D. O. Dumcenco, Y. S. Huang and K. Suenaga, *Nat. Nanotechnol.*, 2014, **9**, 391–396.
10 B. J. Smith and W. R. Dichtel, *J. Am. Chem. Soc.*, 2014, **136**, 8783–8789.
11 H. Sen Xu, S. Y. Ding, W. K. An, H. Wu and W. Wang, *J. Am. Chem. Soc.*, 2016, **138**, 11489–11492.
12 C. Liu, Y. Jin, Z. Yu, L. Gong, H. Wang, B. Yu, W. Zhang and J. Jiang, *J. Am. Chem. Soc.*, 2022, **144**, 12390–12399.
13 P. F. Wei, M. Z. Qi, Z. P. Wang, S. Y. Ding, W. Yu, Q. Liu, L. K. Wang, H. Z. Wang, W. K. An and W. Wang, *J. Am. Chem. Soc.*, 2018, **140**, 4623–4631.
14 N. W. Ockwig, A. P. Co, M. O. Keeffe, A. J. Matzger and O. M. Yaghi, *Science*, 2005, **310**, 1166–1171.
15 H. S. Sasmal, A. Kumar Mahato, P. Majumder and R. Banerjee, *J. Am. Chem. Soc.*, 2022, **144**, 11482–11498.
16 A. M. Evans, L. R. Parent, N. C. Flanders, R. P. Bisbey, E. Vitaku, M. S. Kirschner, R. D. Schaller, L. X. Chen, N. C. Gianneschi and W. R. Dichtel, *Science*, 2018, **361**, 52–57.
17 J. Niu, L. Li, Y. Wang, J. Su, J. Li and X. Wang, *Science*, 2018, **52**, 48–52.
18 B. Zhang, M. Wei, H. Mao, X. Pei, S. A. Alshmimri, J. A. Reimer and O. M. Yaghi, *J. Am. Chem. Soc.*, 2018, **140**, 12715–12719.
19 Z. Yang, H. Chen, S. Wang, W. Guo, T. Wang, X. Suo, D. E. Jiang, X. Zhu, I. Popovs and S. Dai, *J. Am. Chem. Soc.*, 2020, **142**, 6856–6860.
20 S. T. Emmerling, R. Schuldt, S. Bette, L. Yao, R. E. Dinnebier, J. Kästner and B. V. Lotsch, *J. Am. Chem. Soc.*, 2021, **143**, 15711–15722.
21 C. Kang, Z. Zhang, V. Wee, A. K. Usadi, D. C. Calabro, L. S. Baugh, S. Wang, Y. Wang and D. Zhao, *J. Am. Chem. Soc.*, 2020, **142**, 12995–13002.
22 T. Jadhav, Y. Fang, W. Patterson, C. H. Liu, E. Hamzehpoor and D. F. Perepichka, *Angew. Chem. Int. Ed.*, 2019, **58**, 13753–13757.
23 A. Acharjya, P. Pachfule, J. Roeser, F. J. Schmitt and A. Thomas, *Angew. Chem. Int. Ed.*, 2019, **58**, 14865–14870.
24 E. Jin, M. Asada, Q. Xu, S. Dalapati, M. A. Addicoat, M. A. Brady, H. Xu, T. Nakamura, T. Heine, Q. Chen and D. Jiang, *Science*, 2017, **676**, 673–676.

25 Z. Chen, D. Yao, C. Chu and S. Mao, *Chem. Eng. J.*, 2023, **451**, 138489.
26 J. M. Campos-Martin, G. Blanco-Brieva and J. L. G. Fierro, *Angew. Chem. Int. Ed.*, 2006, **45**, 6962–6984.
27 T. Zhou, Y. Zhao, J. W. Choi and A. Coskun, *Angew. Chem. Int. Ed.*, 2019, **131**, 16951–16955.
28 Y. Guo, P. Niu, Y. Liu, Y. Ouyang, D. Li, T. Zhai, H. Li and Y. Cui, *Adv. Mater.*, 2019, **31**, 1–10.
29 Z. Wang, Y. Yang, Z. Zhao, P. Zhang, Y. Zhang, J. Liu, S. Ma, P. Cheng, Y. Chen and Z. Zhang, *Nat. Commun.*, 2021, **12**, 1–8.
30 C. Kang, Z. Zhang, A. K. Usadi, D. C. Calabro, L. S. Baugh, K. Yu, Y. Wang and D. Zhao, *J. Am. Chem. Soc.*, 2022, **144**, 3192–3199.
31 Y. Du, D. Calabro, B. Wooler, Q. Li, S. Cundy, P. Kamakoti, D. Colmyer, K. Mao and P. Ravikovitch, *J. Phys. Chem. C*, 2014, **118**, 399–407.
32 T. Sick, J. M. Rotter, S. Reuter, S. Kandambeth, N. N. Bach, M. Döblinger, J. Merz, T. Clark, T. B. Marder, T. Bein and D. D. Medina, *J. Am. Chem. Soc.*, 2019, **141**, 12570–12581.
33 C. Bin Jin, P. Shi, X. Q. Zhang and J. Q. Huang, *Xinxing Tan Cailiao*, 2022, **37**, 1–24.
34 Y. Zheng, S. Xia, F. Dong, H. Sun, Y. Pang, J. Yang, Y. Huang and S. Zheng, *Adv. Funct. Mater.*, 2021, **31**, 1–10.
35 X. Wu, X. Han, Y. Liu, Y. Liu and Y. Cui, *J. Am. Chem. Soc.*, 2018, **140**, 16124–16133.
36 F. Haase and B. V. Lotsch, *Chem. Soc. Rev.*, 2020, **49**, 8469–8500.
37 M. Higashi, K. Domen and R. Abe, *J. Am. Chem. Soc.*, 2013, **135**, 10238–10241.
38 Y. Choi, H. Kim, G. Moon, S. Jo and W. Choi, *ACS Catal.*, 2016, **6**, 821–828.
39 Y. Hou, Z. Wen, S. Cui, X. Guo and J. Chen, *Adv. Mater.*, 2013, **25**, 6291–6297.
40 X. Wang, J. Park, K. Susztak, N. R. Zhang and M. Li, *Nat. Commun.*, 2019, **10**, 380.
41 Y. Hou, J. Li, Z. Wen, S. Cui, C. Yuan and J. Chen, *Nano Energy*, 2014, **8**, 157–164.
42 T. Sun, J. Song, J. Jia, X. Li and X. Sun, *Nano Energy*, 2016, **26**, 83–89.
43 K. Li, Z. Huang, X. Zeng, B. Huang, S. Gao and J. Lu, *ACS Appl. Mater. Interfaces*, 2017, **9**, 11577–11586.
44 H. Wang, C. Yang, F. Chen, G. Zheng and Q. Han, *Angew. Chem. Int. Ed.*, 2022, **61**, e202202328.
45 Z. Zhou, M. Sun, Y. Zhu, P. Li, Y. Zhang, M. Wang and Y. Shen, *Appl. Catal., B*, 2023, **334**, 122862.
46 W. Zhao, P. Yan, B. Li, M. Bahri, L. Liu, X. Zhou, R. Clowes, N. D. Browning, Y. Wu, J. W. Ward and A. I. Cooper, *J. Am. Chem. Soc.*, 2022, **144**, 9902–9909.
47 T. Xu, Z. Wang, W. Zhang, S. An, L. Wei, S. Guo, Y. Huang, S. Jiang, M. Zhu, Y.-B. Zhang and W.-H. Zhu, *J. Am. Chem. Soc.*, 2024, **146**, 20107–20115.
48 L. Li, L. Xu, Z. Hu and J. C. Yu, *Adv. Funct. Mater.*, 2021, **31**, 2106120.
49 Y. Yang, J. Kang, Y. Li, J. Liang, J. Liang, L. Jiang, D. Chen, J. He, Y. Chen and J. Wang, *New J. Chem.*, 2022, **46**, 21605–21614.
50 X. Di, X. Lv, H. Wang, F. Chen, S. Wang, G. Zheng, B. Wang and Q. Han, *Chem. Eng. J.*, 2023, **455**, 140124.
51 P. Das, G. Chakraborty, J. Roeser, S. Vogl, J. Rabeah and A. Thomas, *J. Am. Chem. Soc.*, 2023, **145**, 2975–2984.
52 X. Zhang, J. Zhang, J. Miao, X. Wen, C. Chen, B. Zhou and M. Long, *Chem. Eng. J.*, 2023, **466**, 143085.
53 Q. Zhi, W. Liu, R. Jiang, X. Zhan, Y. Jin, X. Chen, X. Yang, K. Wang, W. Cao, D. Qi and J. Jiang, *J. Am. Chem. Soc.*, 2022, **144**, 21328–21336.
54 J. Sun, H. Sekhar Jena, C. Krishnaraj, K. Singh Rawat, S. Abednatanzi, J. Chakraborty, A. Laemont, W. Liu, H. Chen, Y. Liu, K. Leus, H. Vrielinck, V. Van Speybroeck and P. Van Der Voort, *Angew. Chem. Int. Ed.*, 2023, **62**, e202216719.
55 C. Krishnaraj, H. Sekhar Jena, L. Bourda, A. Laemont, P. Pachfule, J. Roeser, C. V. Chandran, S. Borgmans, S. M. J. Rogge, K. Leus, C. V. Stevens, J. A. Martens, V. Van Speybroeck, E. Breynaert, A. Thomas and P. Van Der Voort, *J. Am. Chem. Soc.*, 2020, **142**, 20107–20116.
56 Y. Liu, W.-K. Han, W. Chi, Y. Mao, Y. Jiang, X. Yan and Z.-G. Gu, *Appl. Catal., B*, 2023, **331**, 122691.
57 Y. Luo, B. Zhang, C. Liu, D. Xia, X. Ou, Y. Cai, Y. Zhou, J. Jiang and B. Han, *Angew. Chem. Int. Ed.*, 2023, **62**, e202305355.
58 W.-K. Han, H.-S. Lu, J.-X. Fu, X. Liu, X. Zhu, X. Yan, J. Zhang, Y. Jiang, H. Dong and Z.-G. Gu, *Chem. Eng. J.*, 2022, **449**, 137802.
59 G. Pan, X. Hou, Z. Liu, C. Yang, J. Long, G. Huang, J. Bi, Y. Yu and L. Li, *ACS Catal.*, 2022, **12**, 14911–14917.
60 M. Wu, Z. Shan, J. Wang, T. Liu and G. Zhang, *Chem. Eng. J.*, 2023, **454**, 140121.
61 T. Yang, Y. Chen, Y. Wang, X. Peng and A. Kong, *ACS Appl. Mater. Interfaces*, 2023, **15**, 8066–8075.
62 L. Zhai, Z. Xie, C.-X. Cui, X. Yang, Q. Xu, X. Ke, M. Liu, L.-B. Qu, X. Chen and L. Mi, *Chem. Mater.*, 2022, **34**, 5232–5240.
63 M. G. Schwab, B. Fassbender, H. W. Spiess, A. Thomas, X. Feng and K. Müllen, *J. Am. Chem. Soc.*, 2009, **131**, 7216–7217.
64 J. Bi, W. Fang, L. Li, J. Wang, S. Liang, Y. He, M. Liu and L. Wu, *Macromol. Rapid Commun.*, 2015, **36**, 1799–1805.